Rare Met.
https://doi.org/10.1007/s12598-021-01744-x

RARE METALS

ORIGINAL ARTICLE

Phase transformations and mechanical properties of a Ti36Nb5Zr alloy subjected to thermomechanical treatments

Qing-Kun Meng, Jia-Dong Xu, Huan Li, Chong-Hang Zhao, Ji-Qiu Qi, Fu-Xiang Wei, Yan-Wei Sui, Wen Ma*

Received: 25 December 2020 / Revised: 28 January 2021 / Accepted: 2 February 2021

Abstract Various solid state phase transformations exist in metastable β-type Ti alloys, which can be employed to optimize the mechanical properties. In this paper, synchrotron X-ray diffraction (SXRD) experiments were carried out to study the phase transformations of a Ti36Nb5Zr alloy subjected to different thermomechanical treatments. Furthermore, the correlation between the phase constitutions and the mechanical properties was discussed. The α″ texture formed, and high-density defects were introduced after cold rolling of the solution treated specimen, leading to the decrease in Young's modulus and the increase in strength. The cold-rolled specimens were then annealed at temperatures from 423 to 773 K for 30 min. Both the Young's modulus and strength increased with annealing temperatures increasing up to 673 K, which resulted from the precipitation of the ω and/or α phases. With further increase in annealing temperatures to 773 K, the β → α precipitation replaced the β → ω_{iso} phase transformation, and the density of defects decreased, leading to the decrease in both the Young's modulus and strength. These results provide theoretical basis for the design biomedical Ti alloys with both low Young's modulus and high strength.

Q.-K. Meng, J.-D. Xu, H. Li, J.-Q. Qi, F.-X. Wei, Y.-W. Sui
School of Materials Science and Physics, China University of Mining and Technology, Xuzhou 221116, China

C.-H. Zhao
Department of Materials Science and Chemical Engineering, Stony Brook University, Stony Brook, NY 11794, USA

W. Ma*
Grinm Group Co., Ltd, Beijing 100088, China
e-mail: mawen@grinm.com

Keywords β-type Ti alloys; Phase transformations; Mechanical properties; Thermomechanical treatments; Synchrotron X-ray diffraction

1 Introduction

Metastable β-type Ti alloys have been attracting considerable attention in the field of biomedical implant applications due to their low Young's modulus, high specific strength, excellent corrosion resistance, light weight and superior biocompatibility [1]. Among these properties, Young's modulus is of special importance whose value should be as close as possible to that of human bones [2]. The modulus mismatch between human bones and metallic implants can lead to the so-called stress shielding effect which eventually causes bone loss, implant loosening and premature failure of the implants [3]. In comparison to α and α + β Ti alloys with modulus higher than 100 GPa, the β-type Ti alloys have a much lower Young's modulus of about 50–80 GPa, making it a desirable candidate for implant materials to reduce the stress shielding effect [4]. By now, various β-type Ti alloys have been developed by alloying Ti with nontoxic elements such as Nb, Mo, Ta, Zr and Sn [5–10]. However, the Young's modulus of human bones is about 10–30 GPa, still lower than that of the current β-type Ti alloys [11]. Besides, high strength is also required for biomedical implants to endure complicated stress inside human bodies [12]. These requirements motivate the continuous development of novel metastable Ti alloys with both low modulus and high strength.

The β-type Ti alloys exhibit a martensitic transformation from the body centered cubic (bcc) β phase to the

Published online: 31 May 2021

C-centered orthorhombic α″ martensite during quenching, and the martensitic transformation start temperature (M_s) decreases with the increase in the contents of alloying elements [13, 14]. The β phase can be stabilized to room temperature against α″ martensitic transformation when the concentration of β stabilizers is above the critical value (β_c) [15]. It is generally accepted that the β phase has the lowest Young's modulus among all the phases in β-type Ti alloys [16]. Furthermore, the Young's modulus of β phase is closely related to its phase stability, with the lowest modulus corresponding to the least stable alloy which can be realized by adding β stabilizers as less as possible while keeping single β phase to room temperature [17]. Therefore, most of the current low modulus Ti alloys consist of β stabilizers slightly higher than the β_c [18]. In addition to α″ martensite, another metastable phase, i.e., athermal ω phase (ω_{ath}), usually forms during quenching metastable β phase from high temperatures or during external stress [7, 19]. The ω_{ath} phase forms through a diffusionless mechanism, has a typical size of several nanometers, and keeps an identical composition with the β matrix [20]. On the other hand, the isothermal ω phase (ω_{iso}) usually forms during low-temperature annealing by a coupled diffusional-displacive transformation mechanism [21]. Different from the ω_{ath} phase, the ω_{iso} phase can grow in size by a factor of 10 or more to several tens of nanometers, and the growth of ω_{iso} phase can reject β stabilizers to the surrounding β matrix [22]. At higher annealing temperatures, the ω_{iso} phase either dissolves into β phase or acts as nucleation sites for the formation α phase [23].

The above solid-state phase transformations including α″ martensitic transformation, ω and α precipitation phase transformation can be employed to enhance the mechanical properties of metastable β-type Ti alloys during thermomechanical treatments [24–27]. However, the precipitation of ω and α phases usually causes significant increase in Young's modulus [28]. This is because that the ω and α phases have much higher modulus than the β phase, and the precipitation of ω and α phases leads to the enrichment of β stabilizers in residual β phase. On the other hand, most previous studies on the thermomechanical treatments of low modulus Ti alloys were carried out for alloys with composition above β_c, since the alloys with the β stabilizer concentration below β_c will undergo stress-induced martensitic transformation during loading [29]. These alloys consist of dual β + α″ phases in solution-treated and quenched state, and usually are considered to be not suitable for biomedical applications due to the low yielding stress. As for the alloys with composition below β_c, current researches focus on the aging response of the solution treated microstructure and the thermal stability of α″ martensite [30, 31]. Whereas, the thermomechanical treatments including severe cold deformation and subsequent annealing treatment were seldom performed on these alloys. Recent results indicated that nearly single β phase can be achieved after thermomechanical treatments of dual β + α″ Ti alloys [32, 33]. These alloys exhibited a low modulus due to the low concentration of β stabilizers, together with a high strength due to the defects introduced by the severe cold deformation. However, systematical study on the phase transformations during thermomechanical treatment of β-type Ti alloys with composition below β_c is still lacking by now.

It has been reported that surface effect of phase transformations exists during quenching of β-type Ti alloys, i.e., the α″ martensite formed on the surface region of the sample while the ω_{ath} phase formed in the interior region [34, 35]. It is well known that the conventional X-ray diffraction (CXRD) identifies the phase constituent within 20–30 μm near the surface of the sample. On the other hand, the transmission electron microscopy (TEM) usually characterizes the microstructures of the interior region, as the foils for TEM observations were usually prepared by thinning from both sides. Therefore, the phase constitutions determined from CXRD patterns or TEM might be not the actual case of the entire sample. Besides, the laboratory XRD instrument has a low resolution, which is caused by the relatively greater wavelength of its X-rays and the coexistence of $K_{\alpha1}$ and $K_{\alpha2}$ diffraction patterns. As a result, it is difficult or even impossible to trace the phase transformations in a very small extent due to the overlapping of diffraction peaks of β, α, α″ and ω phases. By contrast, the synchrotron X-rays have the advantages of short wavelength, good monochromaticity, high penetration, low absorption and high resolution, making it an ideal technique to identify the phases in small volume fraction [36–38]. Furthermore, the high-energy synchrotron X-rays with high flux and low absorption can be diffracted in transmission geometry, making it possible to examine the phase constitution of the entire sample [39].

Our previous studies indicate that a Ti36Nb5Zr alloy, with β stabilizer concentration below β_c, shows potentials to exhibit both low modulus and high strength after thermomechanical treatment [8]. However, the systematic investigations on the phase transformations and its effect on the mechanical properties are still lacking. In this paper, synchrotron X-ray diffraction (SXRD) technique was employed to investigate the phase transformations during thermomechanical treatment of the Ti36Nb5Zr alloy. Special attention was focused on the α″ → β reverse martensitic transformation, ω and α precipitation during annealing of the cold rolled specimens. Finally, the effects of the phase constitutions on the mechanical properties were discussed.

2 Experimental

An ingot with a nominal composition of Ti36Nb5Zr (wt%) was fabricated by arc melting in an argon atmosphere using high purity Ti (99.99%), Nb (99.95%) and Zr (99.95%). In order to obtain homogeneous chemical composition, the ingot was remelt four times. The as-cast ingot was hot forged to a billet with a cross-section of 8 mm × 60 mm, then homogenized at 1223 K for 5 h in vacuum, and finally quenched into water. The homogenized billet was cold rolled into a plate with a thickness of ~ 1 mm at a reduction ratio of 87.5%. The plate was cut into specimens for further heat treatment using electrical discharge machining (denoted as CR hereafter). Part of CR specimens was solution treated at 1073 K for 1 h in an evacuated quartz tube, and quenched into water by breaking quartz tubes (denoted as ST hereafter). On the other hand, part of CR specimens was annealed in a tube furnace at different temperatures from 423 to 773 K for 30 min, followed by quenching into water (denoted as CRA hereafter). Uniaxial tensile tests were conducted at a strain rate of 1×10^4 s^{-1} on an Instron 5982 machine. Tensile specimens have a gauge length of 30 mm and a rectangular cross-section of 1 mm × 4 mm, with the rolling direction parallel to the loading axis. A strain extensometer was used to record the strain for accuracy. The Young's modulus and yielding stress were determined from the stress–strain curves. A Rigaku D/max 2550 diffractometer with Cu Kα radiation was used for conventional XRD measurements at an accelerating voltage of 40 kV and a current of 250 mA. A JEOL 2100 microscope operating at 200 kV was employed for TEM characterizations. Thin foils for TEM observations were prepared by a twin-jet electro-polishing technique in a solution of 4% perchloric acid in methanol at about 250 K.

SXRD experiments were conducted at an X-ray powder diffraction beamline (XPD, 28-ID-2) at National Synchrotron Light Source II (NSLS-II), Brookhaven National Laboratory. The X-ray beam with a size of 0.5 mm × 0.5 mm and a wavelength of 0.01932 nm (corresponding to X-ray energy of 64.17 keV) penetrated the samples with the beam direction perpendicular to the rolling plane and the transverse direction of the diffraction image parallel to the rolling direction of the samples, respectively. A large-area amorphous-silicon digital X-ray detector, with 2048 × 2048 pixels and pixel size of 200 μm × 200 μm, was placed behind the sample to collect the two-dimensional (2D) diffraction images. The sample-to-detector distance was calibrated to be 1492.72 mm using a Ni standard. The one-dimensional (1D) SXRD patterns were integrated azimuthally over the entire diffraction rings of the 2D SXRD images using Dioptas software [40].

3 Results and discussion

3.1 Phase constitutions of solution treated and cold-rolled specimens

Figure 1a shows conventional XRD (CXRD) patterns of ST and CR specimens, and the synchrotron XRD (SXRD) pattern of the CR specimen is also given for comparison. As both laboratory and synchrotron X-rays were used in the present paper, the intensities of the XRD patterns were plotted against a wavelength independent parameter, i.e., the reciprocal lattice vector $Q = 2\pi/d$, where d is the interplanar spacing [41]. The alloy consisted of dual β + α″ phases after quenching from single β phase field (i.e., ST state), demonstrating that the β stabilizer concentration of the Ti36Nb5Zr alloy is below β_c. On the other hand, clearly β and α″ diffraction peaks can be identified from the CXRD pattern of the CR specimen. Previous investigations have reported that the stress-induced martensitic transformation would occur during cold deformation of metastable β-type Ti alloys [42, 43]. Therefore, it is assumed that the volume fraction of α″ martensite increased after cold rolling. Interestingly, the $(200)_{\alpha''}$ relative diffraction peak intensity of the CR specimen increases clearly in comparison to that of the ST specimen. Considering that the CXRD measurements were performed in reflection geometry, and the cold-rolled planes were used for characterization, the increase in the $(200)_{\alpha''}$ diffraction intensity reveals that an α″ texture with the $(200)_{\alpha''}$ parallel to the rolling plane formed during cold rolling.

SXRD pattern in Fig. 1a is smoother in comparison to CXRD pattern, and the $(200)_{\alpha''}$ and $(110)_{\beta}$ diffraction peaks can be separated, indicating a higher resolution of SXRD technique. Furthermore, the relative diffraction peak intensities of α″ martensite are lower in SXRD than that in CXRD. As SXRD measurements were performed in transmission geometry, it can identify the phase constitution of the entire sample while CXRD represents the phase constitution in surface region. This implies that more α″ martensite existed in the surface region in comparison to that in the interior region. In other words, surface effect might exist, and thus the SXRD technique is a desirable technique to study the phase transformations during thermomechanical treatment of the present Ti36Nb5Zr alloy. Figure 1b shows 2D SXRD image of CR specimen, and the uneven intensity distribution of $(020)_{\alpha''}$ along different azimuth angles indicates that the alloy has a clear preferential orientation. It is worth noting that the transverse direction (TD) of the 2D SXRD image is parallel to the rolling direction (RD) of the samples in the experimental setup. The maximum of the diffraction intensity of the $(020)_{\alpha''}$ appears at the TD, suggesting the existence of

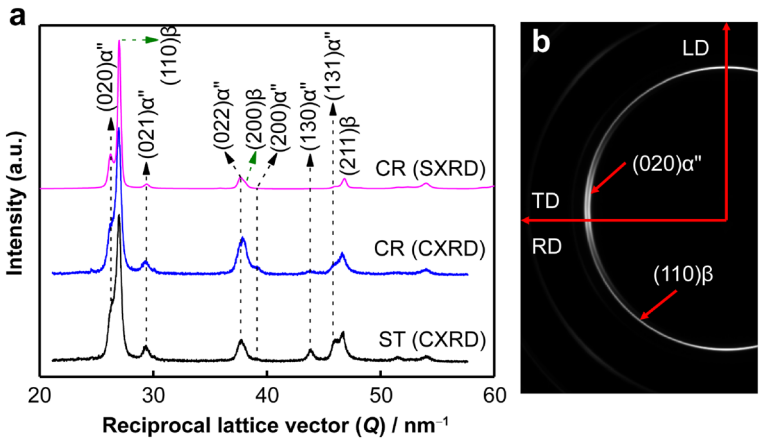

Fig. 1 **a** CXRD and 1D SXRD patterns of solution treated (ST) and cold rolled (CR) specimens; **b** 2D SXRD image of CR specimen (LD, TD and RD in **b** being abbreviations of longitudinal direction, transverse direction and rolling direction, respectively)

texture component with $[020]_{\alpha''}$ crystal direction parallel to RD. Combined with CXRD results, it is proposed that a $(200)_{\alpha''}[020]_{\alpha''}$ martensite texture formed during cold rolling.

3.2 Phase transformations during annealing of cold-rolled specimen

The CR specimens were annealed (CRA) at different temperatures from 423 to 773 K for 30 min and quenched into water. Figure 2 shows 1D SXRD patterns of CRA specimens, and corresponding 2D SXRD images of 6 typical specimens are present in Fig. 3. The phase constitutions of specimens subjected to different thermomechanical treatments were determined from XRD patterns and are given in Table 1. The specimens annealed at temperatures from 423 to 523 K consisted of dual β + α″ phases. The volume fraction of α″ martensite decreased sharply with annealing temperatures increasing, which can be verified by the decrease in the relative $(020)_{\alpha''}$ diffraction peak intensity. It is worth noting that the 523-K annealed specimen consisted of dominant β phase and a trace of α″ phase. The slight amount of martensite was supposed to be caused by the incompletion of reverse martensitic transformation during annealing, rather than the martensitic transformation during quenching. If martensitic transformation occurred slightly during quenching from 523 K, the M_s should be close to room temperature, and stress-induced martensitic transformation would take place during tensile test. However, double yielding phenomenon caused by stress-induced martensitic transformation was only observed in ST specimen, which will be verified in the stress–strain curves. Therefore, a trace of α″ martensite in

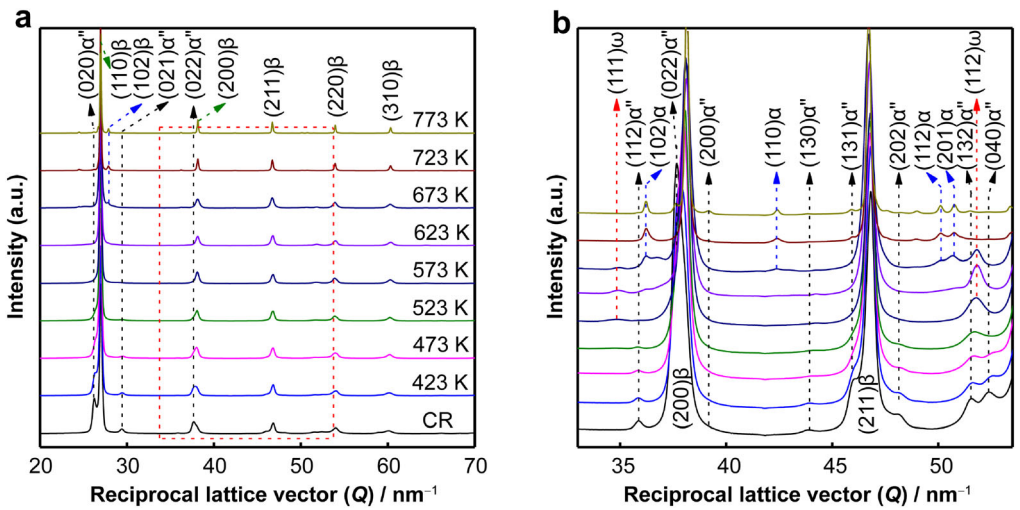

Fig. 2 **a** 1D SXRD patterns of specimens subjected to different thermomechanical treatments; **b** enlarged views of boxed area in **a** (note: intensities being normalized)

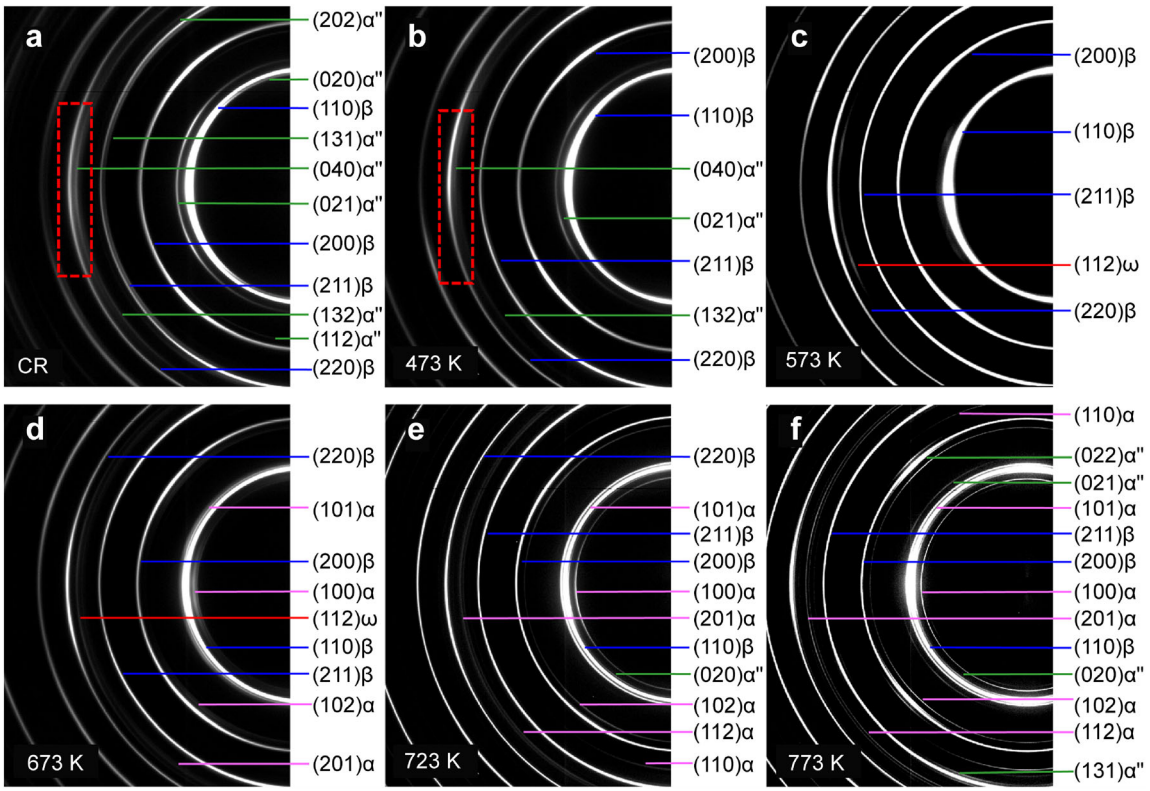

Fig. 3 2D SXRD patterns of **a** CR specimen, and CRA specimens annealed at **b** 473 K, **c** 573 K, **d** 673 K, **e** 723 K and **f** 773 K for 30 min (diffuse zones in position of $(112)_{\omega}$ diffraction rings in **a**, **b** being marked by red rectangles)

Table 1 Phase constitutions determined from XRD patterns

Treatment	Phase constitution
ST	$\beta + \alpha''$
CR	$\beta + \alpha''$
CRA423K, 30 min	$\beta + \alpha''$
CRA473K, 30 min	$\beta + \alpha''$
CRA523K, 30 min	$\beta + \alpha''$
CRA573K, 30 min	$\beta + \alpha''^{a} + \omega$
CRA623K, 30 min	$\beta + \omega + \alpha^{a}$
CRA673K, 30 min	$\beta + \omega + \alpha$
CRA723K, 30 min	$\beta + \alpha + \alpha''$
CRA773K, 30 min	$\beta + \alpha + \alpha''$

[a]Diffraction peaks being very weak

523-K annealed sample resulted from the incompletion of reverse martensitic transformation.

The martensitic transformation is not only closely related to alloy composition, but also sensitive to microstructure [44, 45]. It has been reported that defects such as dislocations, grain boundaries and phase boundaries can suppress the martensitic transformation [46]. The cold rolling introduced high density of dislocations to the present Ti36Nb5Zr alloy and the annealing temperature might be not high enough for complete recrystallization. Besides, the precipitation of ω_{iso} and α phases that can lead to the chemical stabilization of residual β phase was not observed from SXRD patterns for the specimens annealed at temperatures from 423 to 523 K. Therefore, the suppression of martensitic transformation can be attributed to the defects introduced by cold rolling, rather than the chemical composition change of the β phase. By sharp contrast, the ST alloy consisting of dual $\beta + \alpha''$ phases would undergo $\alpha'' \rightarrow \beta$ reverse martensitic transformation upon annealing and $\beta \rightarrow \alpha''$ martensitic transformation upon quenching [30]. As a result, the low-temperature annealing treatment reproduced the initial martensite structure. Apparently, the present thermomechanical treatment is desirable to stabilize low modulus β against α'' martensitic transformation.

At annealing temperatures of 573 and 623 K, diffraction peaks ascribed to $(112)_{\omega}$ appear, and the specimens consisted of dominant β phase and a trace of ω_{iso} phase, as shown in Figs. 2b, 3c and Table 1. Moreover, the $(112)_{\omega}$ diffraction peaks become narrow with annealing temperature increasing, indicating the growth of ω_{iso} particles. The formation of ω_{iso} particles can cause the enrichment of β stabilizers in the residual β phase, which contributed to the suppression of martensite transformation during quenching [47]. Besides, it is believed that high density of dislocations still existed after annealing, which will be verified by the following TEM characterization. As a result, the ω_{iso}

particles, dislocations as well as the chemical stabilization of β matrix led to the decrease of M_s to below room temperature. For the CR specimen and the CRA specimens annealed at temperatures lower than 573 K, diffuse zones can be identified in the position of $(112)_\omega$ diffraction rings from 2D SXRD images, as marked by a red rectangle in Fig. 3a, b. The ω_{ath} phase might form during quenching and cold rolling. After annealing at 423 to 523 K, these ω_{ath} phase might keep unchanged, or transform back to β phase followed by the precipitation of ω_{iso} phase. Therefore, the diffuse zones might be caused by the ω_{ath} phase or the early stages of ω_{iso} phase whose composition is far from equilibrium [20]. The small size and the low volume fraction of the ω particle resulted in diffuse zones instead of clear diffraction rings.

At annealing temperature of 673 K, the relative diffraction peak intensities of ω phase decrease while the diffraction peaks ascribed to α phase appear (Figs. 2b, 3d). It is well known that the precipitation of ω and α phases will compete with each other. The lower temperature and shorter time annealing will prefer the formation of the ω phase while the higher temperature and longer time annealing will be beneficial to the precipitation of the α phase [23, 48]. With the further increase in the annealing temperature to 723 and 773 K, the relative diffraction peak intensities of α phase increase while the diffraction peaks ascribed to ω phase disappear, implying that α precipitation becomes the dominant diffusive phase transformation. Besides, diffraction ring ascribed to $(020)_{\alpha''}$ can be identified from the 2D SXRD image (Fig. 3e) of the 723 K annealed specimen. The relative diffraction peak intensities of α″ martensite become greater at annealing temperature of 773 K (Figs. 2b, 3f), indicating an increased volume fraction. The precipitation of α phase also resulted in the enrichment of β stabilizers in residual β phase, which could contribute to the suppression of martensitic transformation [49]. Meanwhile, the high annealing temperatures led to the considerable decrease in the dislocation density due to recrystallization. As a result, the decrease of M_s caused by the chemical stabilization of the β phase was compensated by the increase of M_s caused by the decrease in the defect density. This might be the reason why M_s was improved to above room temperature after annealing at 723 and 773 K.

Figure 4 shows TEM images of CRA specimens annealed at 573 and 773 K for 30 min. The apparent contrast in Fig. 4a is presumably caused by dislocation tangles, suggesting that complete recrystallization did not occur after 573-K annealing. In other words, high density of defects introduced by the severe cold rolling still existed, verifying that the defects can play an important role in the suppression of martensitic transformation in the 573-K annealed sample. A set of reflections at the 1/3 and 2/3 $\{112\}_\beta$ locations can be easily identified from the selected area diffraction pattern (SADP) of the $<113>_\beta$ zone axis, as shown in Fig. 4b. These reflections should arise from ω_{iso} phase, since ω_{ath} usually exhibits reciprocal lattice streaking and faint additional reflections at 1/3 and 2/3 $\{112\}_\beta$ positions [23]. Using one of the ω reflections marked by white circle in Fig. 4a, b dark-filed TEM image was obtained. It can be seen that the ω_{iso} particles has a small size of several nanometers and is distributed uniformly throughout the β matrix, suggesting that considerable coarsening of the ω_{iso} particles had not occurred after annealing at 573 K.

Figure 4d shows bright-field TEM image of the 773-K annealed specimen. Fine precipitates can be seen in the matrix phase, as marked by the white arrows. The corresponding SADP of the $<110>_\beta$ zone axis in Fig. 4e indicates that the precipitates are α phase, which can be verified by the additional reflections at 1/2 $\{112\}_\beta$ positions. Dark-field TEM image recorded from α reflections marked by the white circle in Fig. 4e is shown in Fig. 4f. It can be seen the fine α precipitates have a plate-like morphology with the length in the scale of one hundred nanometers and width in the scale of ten nanometers. The ω phase was not observed from TEM images, which is consistent with SXRD results in Fig. 2 and verifies that higher annealing temperature prefers the formation of the α phase. However, the α″ martensite was not observed in TEM images for the 773-K annealed specimen, although SXRD results show clear evidence of the presence of the α″ phase. This might be caused by the surface effect of the martensitic transformation during cooling, i.e., martensite only formed on the surface of the sample [35].

3.3 Mechanical properties

Figure 5 shows the uniaxial tensile stress–strain curves and the corresponding Young's modulus of specimens subjected to different thermomechanical treatments. The Young's modulus decreased clearly after cold rolling in comparison to that in ST state. As described above, the α″ texture with [020] crystal direction parallel to RD formed in the CR specimen. It has been reported that the [020] crystal direction processes the lowest Young's modulus among all the crystal directions in α″ phase [12, 44]. Therefore, the decrease in Young's modulus by cold rolling can be ascribed to the elastic modulus anisotropy of α″ martensite as well as the formation of α″ rolling texture. The Young's modulus of specimens annealed at 423 to 523 K kept similar to that of CR specimen, although the volume fractions of α″ martensite decreased considerably with annealing temperatures increasing. Consequently, it is assumed that the Young's modulus of the β phase is close to that of the α″ phase in [020] crystal direction. The Young's modulus increased clearly with the increase in the annealing temperatures from

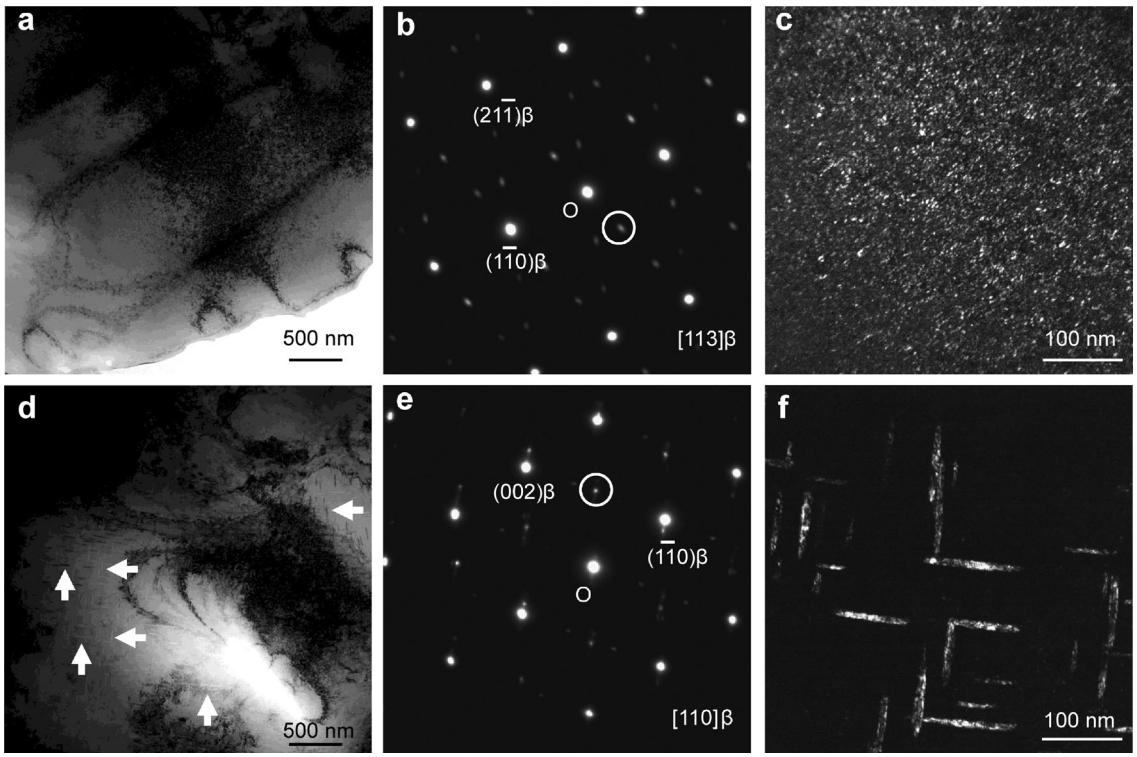

Fig. 4 **a** Bright-field TEM image, **b** corresponding SADP and **c** dark-field TEM image of CRA specimens annealed at 573 K for 30 min; **d** bright-field TEM image, **e** corresponding SADP pattern and **f** dark-field TEM image of CRA specimens annealed at 773 K for 30 min

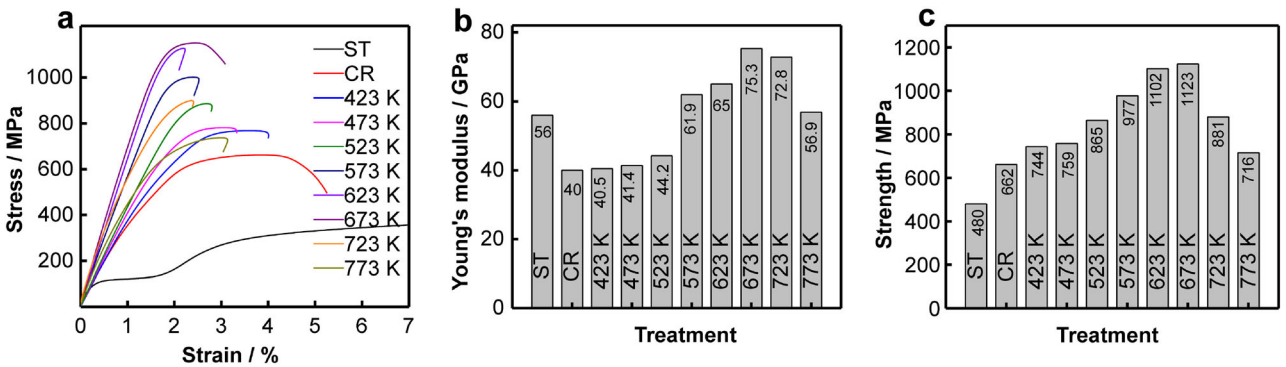

Fig. 5 **a** Tensile stress–strain curves, **b** Young's modulus and **c** UTS of specimens subjected to different thermomechanical treatments (only part of stress–strain curve from 0% to 7% for ST alloy being shown and maximum strain before fracture being about 20%)

523 to 673 K, which apparently resulted from the precipitation of high modulus ω and α phases. Interestingly, the Young's modulus decreased with annealing temperature further increasing to 773 K, although the volume fractions of α phase increased. The ω phase has higher Young's modulus than α phase in Ti alloy [45, 50]. Therefore, the increase in Young's modulus caused by the increasing amount of α phase might be compensated by the decreasing amount of ω phase, leading to the decrease in modulus of specimens annealed at 723 and 773 K.

Figure 5c shows the ultimate tensile strength (UTS) of specimens after different thermomechanical treatments. High density of dislocations was introduced by cold rolling, and thus the strength increased significantly. The UTS increased with annealing temperatures increasing to 523 K, which might be caused by the diffusion of interstitial atoms to the dislocations during recover process. At higher annealing temperatures, the UTS continued to increase and reached maximum value in the specimen annealed at 673 K. The ω_{iso} and α precipitates formed with appropriate annealing temperature, and large amounts of dislocations still existed due to the uncomplete recrystallization process. The interaction between the dislocations and precipitates hindered the movement of dislocations, leading to the

increase in UTS. However, the UTS decreased sharply with the further increase in the annealing temperatures to 773 K. It is proposed that the density of defects decreased considerably at high temperature due to the recrystallization process, which might be the reason for the decrease in the UTS of 723- and 773-K annealed specimens.

It is worth noting that the elongation of the present CR and CRA Ti36Nb5Zr alloy is not enough for practical applications. Severe cold rolling introduced high density of dislocations, and these dislocations still existed after annealing treatments, which might be the main reason for the poor ductility. Furthermore, the formation of ω and/or α phases during cold rolling and annealing treatments led to further decrease in ductility. Finally, the dislocations as well as the precipitates suppressed stress-induced martensitic transformation which can contribute to large elongation during tensile test. Actually, good ductility in many metastable β-type Ti alloys is obtained by the combination of different plastic deformation modes including dislocation slip, stress-induced martensitic transformation, mechanical twinning, etc. [51, 52]. As a solution, better ductility might be achieved by controlling the density of dislocations and the amount of precipitates and by introducing multiple deformation modes. The present work shows promising results that low Young's modulus and high strength can be obtained simultaneously in the Ti36Nb5Zr alloy. It is believed that better combined mechanical properties with good ductility can be realized by adjusting the compositions and thermomechanical treatments.

4 Conclusion

In this paper, the effects of thermomechanical treatments on phase transformations and the mechanical properties of a Ti36Nb5Zr were systematically investigated. The ST and CR alloy consisted of dual β + α″ phases due to the β stabilizer concentration below the β_c. After cold rolling, $(200)_{\alpha''}[020]_{\alpha''}$ texture formed while high density of dislocations was introduced, leading to the decrease in the Young's modulus and the increase in the UTS. After annealing at temperatures from 423 to 523 K for 30 min, the volume fractions of α″ martensite decreased. Meanwhile, the Young's modulus remained almost unchanged and the UTS increased slightly. After annealing at 573 and 623 K for 30 min, the alloy consisted of β and ω_{iso} phases. The ω_{iso} phase grew into a larger size with annealing temperature increasing, leading to the increase in both Young's modulus and UTS. After annealing at 673 K for 30 min, the α phase started to form while the volume fraction of the ω_{iso} phase decreased. The Young's modulus and UTS were further increased to maximum values. After annealing at 723 and 773 K for 30 min, the alloy consisted of β, α and α″ phases. The dissolution of high modulus ω_{iso} phase at high annealing temperatures led to the decrease in Young's modulus.

Acknowledgements This work was financially supported by the Fundamental Research Funds for the Central Universities (No. 2017QNA04). Qing-Kun Meng thanks Prof. Yu-Chen Karen Chen-Wiegart at Stony Brook University and Dr. Jian-Ming Bai, Dr. Hui Zhong and Dr. Sanjit Ghose at National Synchrotron Light Source II for their assistance in the synchrotron experiments. This research used 28-ID-2 (XPD) beamline of the National Synchrotron Light Source II, a U.S. Department of Energy (DOE) Office of Science User Facility operated for the DOE Office of Science by Brookhaven National Laboratory under Contract No. DE-SC0012704.

References

[1] Geetha M, Singh AK, Asokamani R, Gogia AK. Ti based biomaterials, the ultimate choice for orthopaedic implants – a review. Prog Mater Sci. 2009;54(3):397.
[2] Niinomi M. Mechanical biocompatibilities of titanium alloys for biomedical applications. J Mech Behav Biomed Mater. 2008;1(1):30.
[3] Sumner DR, Turner TM, Igloria R, Urban RM, Galante JO. Functional adaptation and ingrowth of bone vary as a function of hip implant stiffness. J Biomech. 1998;31(10):909.
[4] Zhang LC, Chen LY. A review on biomedical titanium alloys: recent progress and prospect. Adv Eng Mater. 2019;21(4):1801215.
[5] Sharma B, Vajpai SK, Ameyama K. Microstructure and properties of beta Ti–Nb alloy prepared by powder metallurgy route using titanium hydride powder. J Alloys Compd. 2016;656:978.
[6] Li BQ, Li CL, Wang ZX, Lu X. Preparation of Ti–Nb–Ta–Zr alloys for load-bearing biomedical applications. Rare Met. 2019;38(6):571.
[7] Wang Q, Wang T, He QX, Wang YY, Wu M. Microstructures and damping properties of Ti-36Nb-2Ta-3Zr-0.3O alloy with different heat treatment temperatures. Chin J Rare Metals. 2019;43(8):785.
[8] Meng Q, Guo S, Ren X, Xu H, Zhao X. Possible contribution of low shear modulus C44 to the low Young's modulus of Ti-36Nb-5Zr alloy. Appl Phys Lett. 2014;105(13):131907.
[9] Li X, Ye S, Yuan X, Yu P. Fabrication of biomedical Ti-24Nb-4Zr-8Sn alloy with high strength and low elastic modulus by powder metallurgy. J Alloys Compd. 2019;772:968.
[10] Jawed SF, Rabadia CD, Liu YJ, Wang LQ, Li YH, Zhang XH, Zhang LC. Beta-type Ti-Nb-Zr-Cr alloys with large plasticity and significant strain hardening. Mater Des. 2019;181:108064.
[11] Niinomi M, Nakai M, Hieda J. Development of new metallic alloys for biomedical applications. Acta Biomater. 2012;8(11):3888.
[12] Matsumoto H, Watanabe S, Hanada S. Microstructures and mechanical properties of metastable β TiNbSn alloys cold rolled and heat treated. J Alloys Compd. 2007;439(1–2):146.
[13] Ramezannejad A, Xu W, Xiao WL, Fox K, Liang D, Qian M. New insights into nickel-free superelastic titanium alloys for biomedical applications. Curr Opin Solid State Mater. 2019;23(6):100783.
[14] Qu WT, Gong H, Wang J, Nie YS, Li Y. Martensitic transformation, shape memory effect and superelasticity of Ti–*x*Zr–(30–*x*)Nb–4Ta alloys. Rare Met. 2019;38(10):965.

[15] Kim HY, Ikehara Y, Kim JI, Hosoda H, Miyazaki S. Martensitic transformation, shape memory effect and superelasticity of Ti–Nb binary alloys. Acta Mater. 2006;54(9):2419.
[16] Tane M, Akita S, Nakano T, Hagihara K, Umakoshi Y, Niinomi M, Mori H, Nakajima H. Low Young's modulus of Ti–Nb–-Ta–Zr alloys caused by softening in shear moduli c′ and c44 near lower limit of body-centered cubic phase stability. Acta Mater. 2010;58(20):6790.
[17] Abdel-Hady M, Hinoshita K, Morinaga M. General approach to phase stability and elastic properties of β-type Ti-alloys using electronic parameters. Scripta Mater. 2006;55(5):477.
[18] Chen LY, Cui YW, Zhang LC. Recent development in beta titanium alloys for biomedical applications. Metals. 2020;10(9):1139.
[19] Nejezchlebová J, Janovská M, Sedlák P, Šmilauerová J, Stráský J, Janeček M, Seiner H. Elastic constants of β-Ti15Mo. J Alloys Compd. 2019;792:960.
[20] Devaraj A, Nag S, Srinivasan R, Williams REA, Banerjee S, Banerjee R, Fraser HL. Experimental evidence of concurrent compositional and structural instabilities leading to ω precipitation in titanium–molybdenum alloys. Acta Mater. 2012;60(2):596.
[21] Ng HP, Devaraj A, Nag S, Bettles CJ, Gibson M, Fraser HL, Muddle BC, Banerjee R. Phase separation and formation of omega phase in the beta matrix of a Ti–V–Cu alloy. Acta Mater. 2011;59(8):2981.
[22] Bönisch M, Calin M, Waitz T, Panigrahi A, Zehetbauer M, Gebert A, Skrotzki W, Eckert J. Thermal stability and phase transformations of martensitic Ti-Nb alloys. Sci Technol Adv Mater. 2013;14(5):055004.
[23] Nag S, Banerjee R, Srinivasan R, Hwang JY, Harper M, Fraser HL. ω-Assisted nucleation and growth of α precipitates in the Ti–5Al–5Mo–5V–3Cr–0.5Fe β titanium alloy. Acta Mater. 2009, 57(7): 2136.
[24] Meng Q, Liu Q, Guo S, Zhu Y, Zhao X. Effect of thermo-mechanical treatment on mechanical and elastic properties of Ti–36Nb–5Zr alloy. Prog Nat Sci. 2015;25(3):229.
[25] Kuroda PAB, Lourenço ML, Correa DRN, Grandini CR. Thermomechanical treatments influence on the phase composition, microstructure, and selected mechanical properties of Ti–20Zr–Mo alloys system for biomedical applications. J Alloys Compd. 2020;812:152108.
[26] Li HJ, Yu Y, Song XY, Ye WJ, Hui SX. Thermal deformation behavior and processing map of a new type of Ti-6554 Alloy. Chin J Rare Metals. 2020;44(5):462.
[27] Lü ZD, Zhang CJ, Du ZX, Han JC, Zhang SZ, Yang F, Chen YY. Relationship between microstructure and tensile properties on a near-β titanium alloy after multidirectional forging and heat treatment. Rare Met. 2019;38(4):336.
[28] Hao YL, Li SJ, Sun SY, Zheng CY, Yang R. Elastic deformation behaviour of Ti–24Nb–4Zr–7.9Sn for biomedical applications. Acta Biomater. 2007, 3(2):277.
[29] Meng Q, Guo S, Liu Q, Hu L, Zhao X. A β-type TiNbZr alloy with low modulus and high strength for biomedical applications. Prog Nat Sci. 2014;24(2):157.
[30] Bönisch M, Panigrahi A, Calin M, Waitz T, Zehetbauer M, Skrotzki W, Eckert J. Thermal stability and latent heat of Nb–rich martensitic Ti-Nb alloys. J Alloys Compd. 2017;697:300.
[31] Mantani Y, Tajima M. Phase transformation of quenched α″ martensite by aging in Ti–Nb alloys. Mater Sci Eng A. 2006;438–440:315.
[32] Meng QK, Huo YF, Ma W, Sui YW, Zhang JY, Guo S, Zhao XQ. Design and fabrication of a low modulus β-type Ti–Nb–Zr alloy by controlling martensitic transformation. Rare Met. 2018;37(9):789.
[33] Guo S, Meng Q, Zhao X, Wei Q, Xu H. Design and fabrication of a metastable β-type titanium alloy with ultralow elastic modulus and high strength. Sci Rep. 2015;5:14688.
[34] Ping DH, Cui CY, Yin FX, Yamabe-Mitarai Y. TEM investigations on martensite in a Ti–Nb-based shape memory alloy. Scripta Mater. 2006;54(7):1305.
[35] Zhu Y, Meng Q, Guo S, Qi L, Xiao W, Ping D, Zhao X. Anomalous phase stability of surface and interior in a metastable Ti-Nb-Zr alloy. Mater Lett. 2016;169:210.
[36] Meng Q, Li H, Wang K, Guo S, Wei F, Qi J, Sui Y, Shen B, Zhao X. In situ synchrotron X-ray diffraction investigations of the nonlinear deformation behavior of a low modulus β-Type Ti36Nb5Zr alloy. Metals. 2020;10(12):1619.
[37] Zhao CH, Kisslinger K, Huang XJ, Lu M, Camino F, Lin CH, Yan HF, Nazaretski E, Chu Y, Ravel B, Liu MZ, Chen-Wiegart YCK. Bi-continuous pattern formation in thin films via solid--state interfacial dealloying studied by multimodal characterization. Mater Horizons. 2019;6(10):1991.
[38] Zhao C, Wada T, DeAndrade V, Gürsoy D, Kato H, Chen-Wiegart Y-cK. Imaging of 3D morphological evolution of nanoporous silicon anode in lithium ion battery by X-ray nano-tomography. Nano Energy. 2018, 52:381.
[39] Lin CH, Topsakal M, Sun K, Bai J, Zhao C, Dooryhee E, Northrup P, Gan H, Lu D, Stavitski E, Chen-Wiegart Y-cK. Operando structural and chemical evolutions of TiS_2 in Na-ion batteries. J Mater Chem A. 2020, 8(25):12339.
[40] Prescher C, Prakapenka VB. DIOPTAS: a program for reduction of two-dimensional X-ray diffraction data and data exploration. High Press Res. 2015;35(3):223.
[41] Ma L, Wang L, Nie Z, Wang F, Xue Y, Zhou J, Cao T, Wang Y, Ren Y. Reversible deformation-induced martensitic transformation in Al0.6CoCrFeNi high-entropy alloy investigated by in situ synchrotron-based high-energy X-ray diffraction. Acta Mater. 2017,128:12.
[42] Chen W, Sun Q, Xiao L, Sun J. Deformation-induced grain refinement and amorphization in Ti-10V-2Fe-3Al alloy. Metall Mater Trans A. 2012;43(1):316.
[43] Yang Y, Li GP, Cheng GM, Li YL, Yang K. Multiple deformation mechanisms of Ti–22.4Nb–0.73Ta–2.0Zr–1.34O alloy. Appl Phys Lett. 2009,94(6):061901.
[44] Matsumoto H, Watanabe S, Hanada S. Beta TiNbSn alloys with low Young's modulus and high strength. Mater Trans. 2005;46(5):1070.
[45] Hao YL, Yang R, Niinomi M, Kuroda D, Zhou YL, Fukunaga K, Suzuki A. Young's modulus and mechanical properties of Ti-29Nb-13Ta-4.6Zr in relation to α″ martensite. Metall Mater Trans A. 2002, 33(10):3137.
[46] Otsuka K, Ren X. Physical metallurgy of Ti–Ni-based shape memory alloys. Prog Mater Sci. 2005;50(5):511.
[47] Kim HY, Fukushima T, Buenconsejo PJS, Nam TH, Miyazaki S. Martensitic transformation and shape memory properties of Ti–Ta–Sn high temperature shape memory alloys. Mater Sci Eng A. 2011, 528(24):7238.
[48] Chou K, Marquis EA. Oxygen effects on ω and α phase transformations in a metastable β Ti–Nb alloy. Acta Mater. 2019;181:367.
[49] de Mello MG, Dainese BP, Caram R, Cremasco A. Influence of heating rate and aging temperature on omega and alpha phase precipitation in Ti35Nb alloy. Mater Charact. 2018;145:268.
[50] Haftlang F, Zarei-Hanzaki A, Abedi HR, Kalaei MA, Nemecek J, Málek J. Room-temperature micro and macro mechanical properties of the metastable Ti–29Nb–14Ta–4.5Zr alloy holding nano-sized precipitates. Mater Sci Eng A. 2020, 771:138583.
[51] Zhu ZW, Xiong CY, Wang J, Li RG, Ren Y, Wang YD, Li Y. In situ synchrotron X-ray diffraction investigations of the physical mechanism of ultra-low strain hardening in Ti-30Zr-10Nb alloy. Acta Mater. 2018;154:45.
[52] Zhang J, Sun F, Chen Z, Yang Y, Shen B, Li J, Prima F. Strong and ductile beta Ti–18Zr–13Mo alloy with multimodal twinning. Mater Res Lett. 2019;7(6):251.